Analytical Potential Energy Formulation for a New Theoretical Approach in Penning Ionization

Stefano Falcinelli[1(✉)], Marzio Rosi[1,2], Franco Vecchiocattivi[1], and Fernando Pirani[3]

[1] Department of Civil and Environmental Engineering, University of Perugia, Via G. Duranti 93, 06125 Perugia, Italy
{stefano.falcinelli,marzio.rosi}@unipg.it, franco@vecchio.it

[2] ISTM-CNR, 06123 Perugia, Italy

[3] Department of Chemistry, Biology and Biotechnologies, University of Perugia, Via Elce di Sotto 8, 06100 Perugia, Italy
fernando.pirani@unipg.it

Abstract. The analysis of recent Penning ionization electron spectra as a function of the collision energy for both Ne^*-Kr and Ne^*-Xe autoionizing reactions allowed the development of a new general theoretical approach able to fully describe the stereodynamics of the Penning ionization reactions at a state to state level. Details on such a general and original approach based on the dependence of the reaction probability on the relative orientation of the atomic and molecular orbitals of reagents and products, are given. The mutual orientation of the collisional partners with respect to the intermolecular axis of the intermediate $[Ne---Rg]^*$ (with Rg = Kr or Xe) excited collision complex (i.e. the transition state of studied reactions) controls the characteristics of the intermolecular potential, which is formulated in a new analytical form whose details are presented and discussed. Obtained results refer to a statistical/random orientation of the open shell ionic core of Ne^*, and in the two cases of Ne^*-Kr and Ne^*-Xe autoionizing collisions, we were able to reproduce and characterize the dependence on the collision energy of the experimental branching ratio between probabilities of spin-orbit resolved elementary processes already published. Such findings result from anisotropy effects connected to atomic orbital orientation/alignment, and their full understanding is a crucial point to describe the dependence of the stereo-dynamics on the electronic structure of the $[Ne---Rg]^*$ transition state. In this way, we are able to fully characterize the state to state reaction probability for the Penning ionization reactions involving Kr and Xe atoms with ionizing Ne^* atoms in either $^3P_2$ and $^3P_0$ sublevels. This original methodology can be applied also to Penning ionization processes involving molecular targets, and in principle is able to point out the basic role of electronic rearrangements inside the transition state of various types of chemical reactions at thermal and sub-thermal collision energies which are of interest in astrochemical environments, being a much more arduous problem in order to be completely characterized.

© Springer Nature Switzerland AG 2019
S. Misra et al. (Eds.): ICCSA 2019, LNCS 11621, pp. 291–305, 2019.
https://doi.org/10.1007/978-3-030-24302-9_21

Keywords: Penning ionization · State to state · Transition state · Electron spectroscopy · Stereodynamics · Metastable atoms

1 Introduction

Penning ionization reactions are elementary processes involving metastable excited species M^* able to ionize atomic or molecular collisional targets X. They can be schematized as it follows:

$$M^* + X \rightarrow [M\text{---}X]^* \rightarrow [M\text{---}X]^+ + e^- \rightarrow \text{final ionic products} \quad (1)$$

where $[M\text{---}X]^*$ and $[M\text{---}X]^+$ are the intermediate neutral and ionic collisional complexes, respectively, being the first the transition state of the reaction [1, 2]. Excited atomic species able to produce Penning ionization are the rare gas atoms excited to their first electronic level as it can be seen from data of Table 1 [3].

Table 1. Main characteristics of the metastable noble-gas atoms.

Atom	Electron configuration	Excitation energy (eV)	Lifetime (s)
$He^*(2^1S_0)$	$1s\ 2s$	20.6158	0.0196
$He^*(2^3S_1)$	$''\ ''$	19.8196	9000
$Ne^*(^3P_0)$	$2p^5\ 3s$	16.7154	430
$Ne^*(^3P_2)$	$''\ ''$	16.6191	24.4
$Ar^*(^3P_0)$	$3p^5\ 4s$	11.7232	44.9
$Ar^*(^3P_2)$	$''\ ''$	11.5484	55.9
$Kr^*(^3P_0)$	$4p^5\ 5s$	10.5624	0.49
$Kr^*(^3P_2)$	$''\ ''$	9.9152	85.1
$Xe^*(^3P_0)$	$5p^5\ 6s$	9.4472	0.078
$Xe^*(^3P_2)$	$''\ ''$	8.3153	150

In fact, metastable rare gas atoms are characterized: (i) by a high energy content ranging from ~8.3 eV for $Xe^*(^3P_2)$ up to ~20.6 (eV) for $He^*(2^1S_0)$ and able to ionize almost all atomic and molecular targets; (ii) by a long lifetime of several seconds allowing them to survive along the typical beam path in the crossed molecular beam experiments (see data of Table 1).

It has to be mentioned that Penning ionization reactions have been widely studied since they are relevant in radiation and plasma chemistry [4, 5], in the laser sources development as well as in combustion [6–9], atmospheric and astrochemistry [10–14] with a particular attention to processes occurring in planetary ionospheres [15–17]. In particular, the relevant role of ionic species in energy generation [18–20] and in space has been pointed out extensively by several review papers to which the interested reader can refer [21–24].

From an experimental point of view, Penning ionization processes are usually studied by crossed molecular beam technique coupled by either mass spectrometry or electron spectroscopy, the first being used to detect the final ions produced by reaction (1), while the latter is applied in order to detect the kinetic energy of emitted electron from the $[M\text{---}X]^*$ autoionizing transition state of such reactions (see Eq. (1)). The cross section for each ionization channel produced by the dynamical evolution of the intermediate $[M\text{---}X]^+$ ionic complex can be measured by mass spectrometry determinations [25, 26], where recently both ion-imaging [27–29] and coincidence techniques [30, 31] have been applied. A real spectroscopy of the transition state can be carried out by analyzing the energy of emitted electrons performing the so called Penning ionization electron spectroscopy (PIES) [32, 33]. A general scheme of a crossed molecular beam experimental apparatus is shown in Fig. 1.

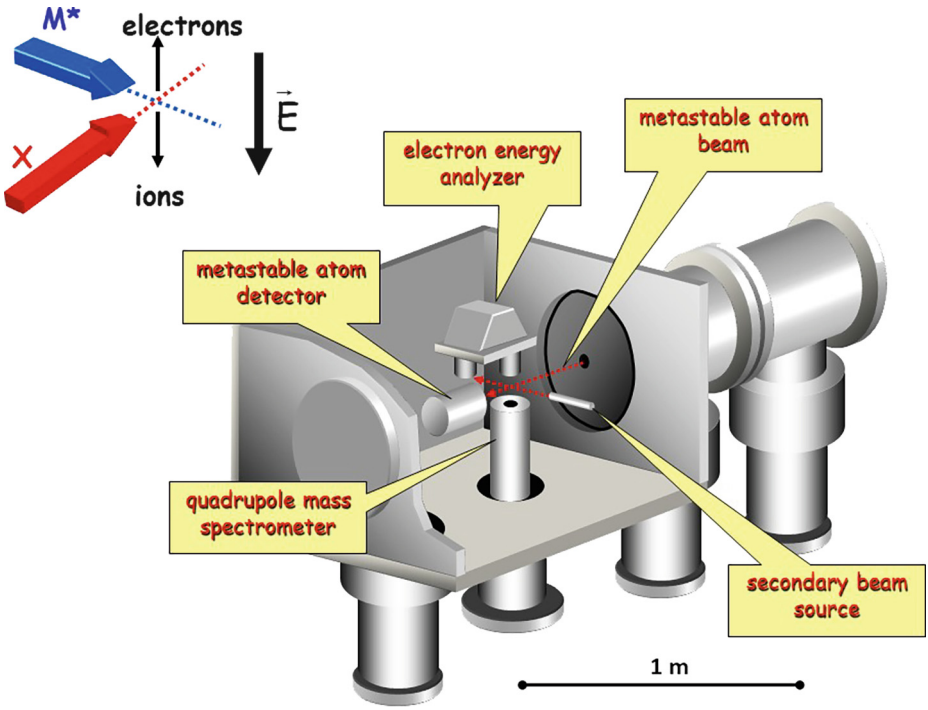


Fig. 1. The general scheme of a crossed molecular beam apparatus for the study of Penning ionization reactions.

From a theoretical point of view, the typical used approach in Penning ionization is based on the so called "Optical Potential Model", first introduced by Bethe for the description of nuclear reacting collisions [34]. It is based on the assumption that the interaction between the colliding partners can be described by a complex potential, and is widely discussed in the next section.

In this paper we report in detail analytical potential energy formulations recently adopted in a new theoretical model describing the microscopic dynamics of simple Penning ionization processes involving Ne^*-Kr and Ne^*-Xe atoms [35–37]. Such a model, thanks to the used Optical Potential Model in which the real part of the potential has been expressed by adopting an Improved Lennard Jones analytical function (see Sect. 3), was able to fully characterize the electron couplings inside the $[Ne\text{---}X]^*$ (where X = Kr or Xe) transition state of autoionizing reaction, reproducing the PIES spectra for both systems and the related branching ratios for the production of final ions in their specific spin-orbit states as a function of the collision energy [35, 36]. In such a way, we were able to formulate a complete description of the stereodynamics of the processes in a state to state picture in terms of adiabatic and non-adiabatic effects [35, 36].

2 The Optical Potential Model

As it is well known, the optical potential W, describing Penning ionization (i.e. autoionization processes), is expressed by a combination of a real part V (depicting the interaction between the two neutral incoming collisional partners) and an imaginary part Γ (quantifying the ionization probability as a function of the internuclear distance R) [38–40]:

$$W = V - i/2\,\Gamma \tag{2}$$

The intensity of both these portions of the global potential depends on: (i) the separation distance, R; (ii) the relative orientation of two involved partners; (iii) and the characteristics of the manifold of quantum states attainable for the system along the collision. As discussed in details in next Sect. 3, such features, by configuration interaction, audit the mix among entrance and exit channels. In the case of Ne^*-Kr and Ne^*-Xe, the two simple atom-atom systems presented in this study, the used radial and angular terms point out the dependence of the potential energy on R and on the half-filled orbital orientation of Ne^*, respectively.

3 The Potential Energy Formulation

The real V component of the optical potential model of Eq. (2) can be formulated phenomenologically using the following Eq. (3):

$$V_t(R) = S(R)V(R)^{neut.-neut.} + (1 - S(R))V(R)^{ion-neut.} \tag{3}$$

where $V(R)^{neut.-neut.}$ and $V(R)^{ion-neut.}$ represents the interaction between the incoming neutral collision partners $[Ne\text{---}Rg]^*$ (where Rg = Kr or Xe) before the ionization and that between outcoming ionic states $[[Ne\text{---}Rg]^+$ after the autoionization, respectively. Either potential energy formulations have been depicted using the Improved Lennard Jones function widely applied in a number of cases [41–45], whose general form is the following:

$$V_{ILJ}(R) = \varepsilon \left[\frac{m}{n(R) - m} \left(\frac{R_m}{R} \right)^{n(R)} - \frac{n(R)}{n(R) - m} \left(\frac{R_m}{R} \right)^{m} \right] \tag{4}$$

where

$$n(R) = \beta + 4 \left(\frac{R}{R_m} \right)^2 \tag{5}$$

In Eq. (4), ε stands for the potential well depth whereas R_m quantify its location in Å; $n(R)$ fixes the repulsive wall with its hardness, and the radial modulation of the attractive interaction. $S(R)$ in Eq. (3) is a switching function accounting for the transition between the neutral-neutral and the ion-neutral formulation, as previously adopted to describe the collisional interaction for other systems [39, 46–51]. Such a switching function has been defined by Eq. (6) below:

$$S(R) = \frac{1}{1 + e^{\left(\frac{R_o - R}{d}\right)}} \tag{6}$$

In this formulation, the internuclear distance where the two combined limiting potential forms have the same weight is indicated as R_o, and the d parameter accounts for the rapidity of the transition. It has to be noted that, in general, in order to carry out a complete representation of the real V component of Eq. (2) it is required to consider two additional features:

(i) At large internuclear distance R, the ILJ formulation of the interaction potential appears to be complete; in fact, where R is large, the neutral-neutral interaction is prevailing and the collisional system is characterized by a substantial isotropic behavior which is typical of the interaction between an alkaline atom and a noble gas partner.
(ii) At short R distances, it is required to consider anisotropic contributions due to the open shell nature of the metastable atom because the role of its ionic core is coming out [52].

In our laboratory where developed guidelines to model such interactions [53, 54], giving us a powerful and reliable means to describe the interaction energy when an open "P" shell atom approaches a closed shell species. This can be done employing effective adiabatic potential energy curves, including contributions associated to pure Σ and Π molecular states: they are defined by the Λ = 0 and Λ = 1 electronic quantum number and are picked out as V_Σ and V_Π, mixed by spin-orbit effects. A weighted sum of V_0 an V_2 Legendre radial terms, defined as $V_0 = (V_\Sigma + 2V_\Pi)/3$ and $V_2 = 5(V_\Sigma - V_\Pi)/3$ has been properly adopted for such a description. We can also formulate the related inverse relations as $V_\Sigma = V_0 + 2/5V_2$ and $V_\Pi = V_0 - 1/5V_2$. By this procedure, the V_0 term accounts for the spherical average of the interaction component, while all anisotropic contributions, which derive from quantized spatial orientations of the valence orbitals of the open shell atom within the interacting collisional complex, are evaluated by the V_2 anisotropic term employment. When we consider the case of

collisions involving ^2P_J (or ^3P_J) open shell atoms, as is the case of Ne^+ (or Ne^*) and Kr^+, Xe^+ ions with a inverted sequence of spin-orbit sublevels, it is possible to formulate the effective adiabatic potential energy curves $V_{|J,\Omega>}$ (where Ω is the quantum number fixing the absolute projection of **J** along R) by the following Eqs. (7)–(9):

$$V_{|3/2,3/2>} = V_0 - \frac{1}{5}V_2 \tag{7}$$

$$V_{|3/2,1/2>} = V_0 + \frac{1}{10}V_2 + \frac{1}{2}\Delta - \frac{1}{2}\left(\frac{9}{25}V_2^2 + \Delta^2 - \frac{2}{5}V_2\Delta\right)^{1/2} \tag{8}$$

$$V_{|1/2,1/2>} = V_0 + \frac{1}{10}V_2 + \frac{1}{2}\Delta + \frac{1}{2}\left(\frac{9}{25}V_2^2 + \Delta^2 - \frac{2}{5}V_2\Delta\right)^{1/2} \tag{9}$$

In Eqs. (8) and (9) above, the Δ parameter represents the energy splitting between J = 1/2 and J = 3/2 atomic sublevels. In the case of Ne^+, we have $\Delta = 0.097$ eV; when we consider Kr^+, we have $\Delta = 0.665$ eV; and for Xe^+, results $\Delta = 1.306$ eV. Furthermore, in all three Eqs. (7)–(9) the V_0 term (both in the entrance and exit channel cases) has been formulated adopting the ILJ function defined by Eqs. (3)–(5) above. On the other hand, the use of an exponential decreasing function (determined by a pre-exponential factor A, and by a proper α exponent) allowed us to obtain a reliable representation of the V_2 term. All the used parameters for the accurate potential energy description of the two Ne^*-Kr and Ne^*-Xe autoionizing systems are given in Table 2 below.

Table 2. The Potential parameters of the real part of the formulated Optical Potential Model, V (see Eq. (2) and text) adopted in the description of the two investigated Ne^*-Kr and Ne^*-Xe autoionizing systems.

System	Isotropic component					Anisotropic component	
	ε (meV)	R_m (Å)	β	R_0 (Å)	d (Å)	A (meV)	α (Å^{-1})
Ne^*-Kr	9.0	5.18	6.7	3.85	0.55		
Ne^+-Kr	209.0	2.86	8.0			1.674×10^7	4.32
Ne-Kr^+	33.7	3.08	9.0				
Ne^*-Xe	13.8	5.22	6.7	3.85	0.55		
Ne^+-Xe	268.6	3.02	8.0			2.511×10^7	4.32
Ne-Xe^+	28.4	3.27	8.0				

It has to be noted that in the Ne^*-Rg (where Rg = Kr and Xe) autoionizing collisional systems, all involved potential energy curves are affected by a bond stabilization by Charge Transfer V_x, whose strength is depending by the coupling of the configuration interaction between quantum states having the same symmetry and differing for one electron exchange. This is a consequence of the fact that internal quantum states in both $(Ne\text{-}Kr)^+$ and $(Ne\text{-}Xe)^+$ ionic adducts should be the same of noble gas-halide systems. Furthermore, it has been also established [53, 54] that the term V_2 for such

systems must be fixed equal to $\frac{5}{2} V_x$. Consequently, it happens that $V_2 < 0$, for the lower Ne-Kr^+ and Ne-Xe^+ quantum states, whereas $V_2 > 0$ for the upper Ne^+-Kr, and Ne^+-Xe states. This status is due to *bonding and antibonding* effects which appears between states of the same symmetry, even in the perturbation limit. Besides, such a kind of interaction potential analytical expression leads to a diverse correlation between atomic states, which represent the collisional system at a long range of internuclear separation distances R, where $|V_2| \ll \Delta$, and molecular states of the same system arising at short R range, where $|V_2| \gg \Delta$. Furthermore, it has been also pointed out that both Σ and Π characters of implicated potential energy curves $V_{|J,\Omega>}$ at all R values, can be formulated by the following Eqs. (10)–(12) [55, 56]:

$$V_{|3/2,1/2>} = cos^2\alpha V_\Sigma + sin^2\alpha V_\Pi \tag{10}$$

$$V_{|1/2,1/2>} = sin^2\alpha V_\Sigma + cos^2\alpha V_\Pi \tag{11}$$

where

$$\cos^2\alpha = \frac{1}{2} + \frac{\left(1 - \frac{9V_2}{5\Delta}\right)}{4\sqrt{2}\sqrt{1 + \left[\left(\frac{1-\frac{9V_2}{5\Delta}}{2\sqrt{2}}\right)\right]^2}} \tag{12}$$

Such equations are in agreement with the following asymptotic conditions: (i) at short R internuclear distances, all potential energy curves should account for quantum states having a pure Σ or Π character; (ii) at large R distances, where is prevailing the spin-orbit coupling, a mixing of the two characters occurs. Furthermore, it has to be noted that the different behavior of Ne^+-Kr and Ne^+-Xe with respect to Ne-Kr^+ and Ne-Xe^+, respectively, results from the opposite sign of V_2 potential term and from the different role played by the spin-orbit mixing, fixed by different Δ values. Since the character of $V_{|3/2,3/2>}$ term shows a pure Π character at all internuclear distances R, the behavior of its related curves is not discussed in detail. It must be considered that has been already proved [57] that non adiabatic effects (which are promoted by changes in the electronic angular coupling schemes describing the transition from atom-atom to molecular states) play their crucial role with the highest probability at a R distance where $|V_2|$ is comparable with Δ.

In the data analysis of PIES spectra recorded as a function of the collision energy for the two autoionizing Ne^*-Kr and Ne^*-Xe systems, already published [35, 36], it has been assumed that the population of the Ne^* reagent atoms in their $^3P_2$ fine spin-orbit level is 5 times higher than $^3P_0$ (see also next section). Furthermore, we defined as x the Σ character degree in the entrance channels, while in the exit ones it is indicated as y, and consequently the Π character degree of each state has indirectly obtained from the Σ one. After that, we determined the $A_{\Pi-\Pi}/A_{\Sigma-\Sigma}$ and $A_{\Pi-\Sigma}/A_{\Sigma-\Pi}$ ratios adopted to fix the relative role of the two proposed microscopic mechanisms of investigated autoionization reactions in terms of adiabatic and non-adiabatic effects. These data have been recently published [35, 36], has been fixed to the same value of $f = 0.2$, following the proper suggestion by Krauss [58]. All such assumptions drove us to the formulation

of eight coefficients, expressed by Eqs. (13)–(20) below, which account for both the character of symmetry and the degeneracy of all allowed quantum states, as well as for the value of *f*. Their analytical definition is the following:

$$A = [(1-x)y + f(1+x)(2-y)] \tag{13}$$

$$B = [xy + f(1-x)(2-y)] \tag{14}$$

$$C = [(1-x)(2-y) + f(1+x)y] \tag{15}$$

$$D = [x(2-y) + f(1-x)y] \tag{16}$$

$$E = [x(1-y) + f(1-x)y] \tag{17}$$

$$F = [xy + f(1-x)(1-y)] \tag{18}$$

$$G = [(1-x)(1-y) + f(1+x)y] \tag{19}$$

$$H = [(1-x)y + f(1+x)(1-y)] \tag{20}$$

A, B, C, D, E, F, G, and H coefficients enable us to quantify the relative height H_i of the peaks in the PIES, measured in Ne^*-Kr and Ne^*-Xe autoionizing collisions at the same collision energy for each channel $i = a, b, c$ respect to the reference one, that in the present cases corresponds to the $^3P_0$-$^2P_{3/2}$ reactive channel, with the relative value of $A_{\Sigma-\Sigma}$ and $A_{\Sigma-\Pi}$ probability terms (see next section). In particular, the performed analysis has been done adopting the following Eq. (21):

$$A_{\Sigma-\Pi} = \frac{H_a - \frac{5}{2}\frac{A}{B}}{\frac{1}{2}\left\{-\frac{DA}{B} + C\right\}} \quad \text{and} \quad A_{\Sigma-\Sigma} = \frac{1 - \frac{1}{5}DA_{\Sigma-\Pi}}{\frac{1}{5}B} \tag{21}$$

where H_a represents the relative height of the $^3P_2$-$^2P_{3/2}$ PIES peak. In a consistent way, the relative heights of other Ne^*-Kr and Ne^*-Xe PIES peaks have been formulated by Eq. (22) below:

$$H_b = (A_{\Sigma-\Sigma}E + A_{\Sigma-\Pi}F)\frac{1}{5} \quad \text{and} \quad H_c = (A_{\Sigma-\Sigma}G + A_{\Sigma-\Pi}H)\frac{1}{2} \tag{22}$$

where *b* and *c* are related to the $^3P_0$-$^2P_{1/2}$ and $^3P_2$-$^2P_{1/2}$ reactive channels, respectively.

Different collision energies, representative of low, intermediate and high values in the ranges probed by the experiments, have been investigated in detail reproducing and fully describing in a consistent way the obtained experimental results for both studied Ne^*-Kr and Ne^*-Xe autoionizing atom-atom systems, as it is summarized in next

section. This demonstrated that the proposed analytical formulation of the Optical Potential Model proposed in this paper, and discussed in detail above, is a new and original theoretical approach to give a reliable general description of the interaction between the autoionizing collisional partners in Penning ionization reactions. The reader interested to a complete description of the analysis applied to PIES spectra recorded in Ne^*-Kr and Ne^*-Xe experiments, and based on the potential energy formulation here presented, can refer to two recent publications by our group [35, 36]. In next section, only a brief description of such an analysis is given just to provide, for completeness of exposition, some proof of the reliability of the analytical method used to describe the interaction in collisional autoionization processes.

4 The Ne^*-Kr and Ne^*-Xe PIES Spectra

As already mentioned, recent PIES experiments performed for both Ne^*-Kr and Ne^*-Xe autoionizing systems [35, 36, 54] are consistent each other and confirm the suitability of the original methodology in the formulation of the Optical Potential Model of Eq. (2), fully described in detail in Sect. 3. In this section we recall only the main steps of the adopted methodology used in the analysis of PIES spectra, as an example of the reliability of our proposed theoretical model, whose complete analytical formulation has been given in Sect. 3. The interested reader to a complete overview of recent applications of our theoretical approach in modeling the interaction potential for Penning ionization can found details in the literature [35, 36].

The recorded PIES spectra in Ne^*-Kr and Ne^*-Xe as a function of the collision energy, and used to test the reliability of the analytical potential energy formulation here presented, are shown in Fig. 2. They demonstrate that electron spectra are composed by four contributions arising from four different channels associated with the two different spin-orbit states of the $Ne^*(^3P_{2,0})$ reactant and to the two spin-orbit states of Kr^+ and Xe^+ ($^2P_{3/2,1/2}$) products (see panels reported in Fig. 2).

In order to obtain the relative probability of the four channels, we have fitted the Ne^*-Kr PIES at the lowest investigated collision energy (where the recorded signal to noise ratio was the best, minimizing the experimental error [35, 59]) using four Gaussian functions, whose general analytical expression is the following:

$$y(x) = Hexp^{\left(\frac{B-x}{C}\right)^2} \tag{23}$$

By imposing to the four used Gaussian functions the same width (expressed by the coefficient C) and the same relative peak position (i.e. the B change, defined according to the spin-orbit separation of Ne^*) we carried out the fitting of PIES spectra recorded at

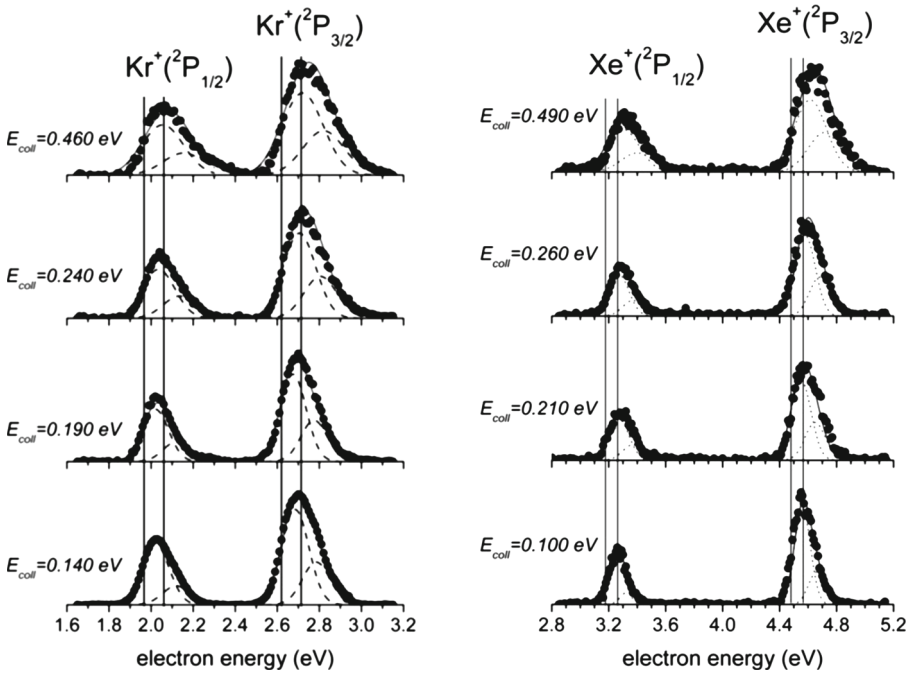


Fig. 2. The PIES spectra for the ionization of Kr and Xe by Ne^* atoms measured as a function of the collision energy and for resolution conditions of about 80 meV. Their comparison emphasizes the dependence of the relative role of the four channels (see text), obtained by the variation of the relative height of the four Gaussian functions, and of the peak positions with the collision energy.

each investigated collision energy. By such a procedure we were able to refer the relative probability of the four different reactive channels to the relative height of the four PIES peaks, obtainable from the ratio of H parameter values. Although the Gaussian functions are symmetric, their combination supplied an asymmetric frame of the simulated global peak. This accounted for the shoulders observed in the right hand of each peak position (see Fig. 2). The parameters of the Gaussian functions used in the best-fitting procedure have been reported in Table 3. As a deeper test and further generalization of such a methodology, the same group of four Gaussian functions has been employed in the description of all PIES reported in Fig. 2, and recorded at higher collision energies: only their width has been adjusted (increased) to take into account for the reduced electron energy resolution conditions used in such measurements at higher collision energies (see the variation of the C parameter in Table 3 below).

Table 3. The parameters of Gaussian functions $f(x) = Hexp\left[\left(\frac{B-x}{C}\right)^2\right]$ exploited for describing the Penning ionization electron energy spectra of the state to state ionization reactions, $Ne^*(^3P_{Ji}) + Kr(^1S_0) \rightarrow Ne(^1S_0) + Kr^+(^2P_{Jf}) + e^-$ (see text).

Collision energy (eV)	$J_i \rightarrow J_f$ transition	H (arb. units)	B (eV)	C (eV)	$H_{J_i \rightarrow J_f}/H_{0 \rightarrow 3/2}$
0.140	2 → 1/2	0.500	2.020	0.092	1.43
	0 → 1/2	0.155	2.120	0.092	0.44
	2 → 3/2	0.780	2.685	0.092	2.23
	0 → 3/2	0.350	2.785	0.092	1.00
0.190	2 → 1/2	0.450	2.020	0.088	1.27
	0 → 1/2	0.170	2.120	0.088	0.48
	2 → 3/2	0.750	2.675	0.088	2.11
	0 → 3/2	0.355	2.775	0.088	1.00
0.240	2 → 1/2	0.420	2.035	0.110	1.17
	0 → 1/2	0.190	2.135	0.110	0.53
	2 → 3/2	0.730	2.705	0.110	2.03
	0 → 3/2	0.360	2.805	0.110	1.00
0.460	2 → 1/2	0.410	2.055	0.139	1.13
	0 → 1/2	0.180	2.155	0.139	0.50
	2 → 3/2	0.670	2.720	0.139	1.85
	0 → 3/2	0.362	2.820	0.139	1.00

In this latter case the shoulders in the PIES peaks are less evident. Furthermore, the relative probability of the four state to state Ne^*-Kr and Ne^*-Xe reactions where determined from the data analysis, adopting the same methodology presented above to reproduce measured PIES peaks with their asymmetry. The left panel of Fig. 2 shows the PIES measured for Ne^*-Kr at different collision energies, and with their fit performed by the use of four Gaussian functions, always imposing the same boundary conditions as stressed above. As an example, the related used fit parameters only for the case of Ne^*-Kr autoionizing collisions are reported in Table 3. As indicated above, an internally consistent procedure applied at each collision energy allowed to obtain the ratio of the H parameter values of Table 3, providing the relative probability of the four reactive channels. In particular, in our procedure the $^3P_0$-$^2P_{3/2}$ reactive channel was chosen as the reference one, and values of the relative probability for the other channels, given in Table 3, have been so extracted. Their dependence on the collision energy has been determined also in the case of Ne^*-Xe system (whose PIES spectra are shown in the right panel of Fig. 2) adopting the same procedure described for Ne^*-Kr, and demonstrating the existence of an internally consistent behavior between the two autoionizing systems. The reader can found details on both the used best-fitting procedure and the related fit parameters also for the case of Ne^*-Xe system in recent publications [35, 36]. By this adopted model the dependence of the peak height ratio on the collision energy allowed us to extract information on the relative role of the two mechanisms for Penning ionization reactions that we have recently classified as

Table 4. Two different sequences of the Σ character, whose values, defined as x in the entrance channels and y in the exit channels. The Π character of each state has indirectly obtained from the Σ one. The error in the P_2/P_0 ratio has been estimated by the uncertainty in the measured peak height.

Energy range	P_2/P_0 ratio	Sequence 1		Sequence 2	
		x	y	x	y
High	1.85 ± 0.09	0.85	0.73	0.90	0.74
Intermediate	2.12 ± 0.11	0.75	0.70	0.80	0.71
Low	2.82 ± 0.15	0.60	0.67	0.60	0.67

"indirect" or "direct" mechanism in terms of adiabatic and non-adiabatic effects, respectively [35]. The relative role of such two mechanisms is defined as $A_{\Sigma\text{-}\Pi}/A_{\Sigma\text{-}\Sigma}$ ratio, by taking into account: (i) the radial dependence of both Σ and Π characters, associated to the entrance and exit channels; (ii) the relative population $^3P_0/^3P_2$ of Ne^* amounting to a 1/5 ratio, according to a statistical distribution of fine structure sublevels. As already mentioned above, all the explicit equations used to achieve this purpose are those already reported and discussed in Sect. 3 (see, in particular, Eqs. (21) and (22)) and constitute a new and original theoretical method for modeling the Optical Potential (see Eq. (2)) in a general and analytical form. In our procedure, we have also applied the same methodology assuming two different sequences of Σ and Π character (see Table 4), having all values confined within the estimated uncertainty band, in order to characterize the relative role of the two adiabatic and non-adiabatic mechanisms (see above) with its collision energy dependence.

5 Conclusions

In this paper, we presented a new analytical formulation for the potential energy describing the interaction in typical atom-atom autoionizing systems, as Ne^*-Kr and Ne^*-Xe. Obtained results refer to a statistical/random orientation of the open shell ionic core of $Ne^*(^3P_{2,0})$ and in the two investigated cases (the Ne^*-Kr and Ne^*-Xe autoionizing collisions) we were able to characterize the dependence on the collision energy of the PIES spectra and of the relative experimental branching ratio between probabilities of spin-orbit resolved elementary processes already published.

This new and original methodology can be applied also to Penning ionization processes involving molecular targets already studied experimentally in our laboratory [60, 61], and in principle is able to point out the basic role of electronic rearrangements inside the transition state of various types of reactions at thermal [62–65] and subthermal collision energies which are of interest also in astrochemical environments [66–69], being a much more arduous problem in order to be completely characterized.

Acknowledgments. This work is dedicated to our colleague and friend Jaime De Andres whose memory and love for science will inspire our future research. Financial support from MIUR, "Ministero dell'Istruzione, dell'Università e della Ricerca", PRIN 2015 (STARS in the CAOS-Simulation Tools for Astrochemical Reactivity and Spectroscopy in the Cyberinfrastructure for Astrochemical Organic Species, 2015F59J3R). Support from Italian MIUR and University of Perugia (Italy) is acknowledged within the program "Dipartimenti di Eccellenza 2018–2022".

References

1. Benz, A., Morgner, H.: Mol. Phys. **57**, 319–336 (1986)
2. Falcinelli, S., Bartocci, A., Cavalli, S., Pirani, F., Vecchiocattivi, F.: Chem. Eur. J. **22**(2), 764–771 (2016)
3. Falcinelli, S., et al.: Modeling the intermolecular interactions and characterization of the dynamics of collisional autoionization processes. In: Murgante, B., et al. (eds.) ICCSA 2013. LNCS, vol. 7971, pp. 69–83. Springer, Heidelberg (2013). https://doi.org/10.1007/978-3-642-39637-3_6
4. Falcinelli, S., Capriccioli, A., Pirani, F., Vecchiocattivi, F., Stranges, S., Martì, C., et al.: Fuel **209**, 802–811 (2017)
5. Falcinelli, S., Rosi, M., Cavalli, S., Pirani, F., Vecchiocattivi, F.: Chem. Eur. J. **22**(35), 12518–12526 (2016)
6. Cavallotti, C., Leonori, F., Balucani, N., Nevrly, V., Bergeat, A., et al.: J. Phys. Chem. Lett. **5**, 4213–4218 (2014)
7. Leonori, F., Balucani, N., Nevrly, V., Bergeat, A., et al.: J. Phys. Chem. C **119**(26), 14632–14652 (2015)
8. Leonori, F., Petrucci, R., Balucani, N., Casavecchia, P., Rosi, M., Berteloite, C., et al.: Phys. Chem. Chem. Phis. **11**, 4701–4706 (2009)
9. Leonori, F., Petrucci, R., Balucani, N., Hickson, K.M., Hamberg, M., Geppert, W.D., et al.: J. Phys. Chem. A **113**, 4330–4339 (2009)
10. Rosi, M., Falcinelli, S., Balucani, N., Casavecchia, P., Leonori, F., Skouteris, D.: Theoretical study of reactions relevant for atmospheric models of titan: interaction of excited nitrogen atoms with small hydrocarbons. In: Murgante, B., et al. (eds.) ICCSA 2012. LNCS, vol. 7333, pp. 331–344. Springer, Heidelberg (2012). https://doi.org/10.1007/978-3-642-31125-3_26
11. Alagia, M., et al.: Chem. Phys. Lett. **432**, 398–402 (2006)
12. Alagia, M., et al.: J. Phys. Chem. A **113**, 14755–14759 (2009)
13. Alagia, M., et al.: Phys. Chem. Chem. Phys. **12**, 5389–5395 (2010)
14. Falcinelli, S., Pirani, F., Alagia, M., Schio, L., Richter, R., et al.: Chem. Phys. Lett. **666**, 1–6 (2016)
15. Falcinelli, S., Pirani, F., Vecchiocattivi, F.: Atmosphere **6**(3), 299–317 (2015)
16. Biondini, F., Brunetti, B.G., Candori, P., De Angelis, F., et al.: J. Chem. Phys. **122**(16), 164307 (2005)
17. Biondini, F., Brunetti, B.G., Candori, P., De Angelis, F., et al.: J. Chem. Phys. **122**(16), 164308 (2005)
18. Nicolaides, C.A.: Chem. Phys. Lett. **161**(6), 547–553 (1989)
19. Falcinelli, S., Fernandez-Alonso, F., Kalogerakis, K., Zare, R.N.: Mol. Phys. **88**(3), 663–672 (1996)
20. Tosi, P., Correale, R., Lu, W., Falcinelli, S., Bassi, D.: Phys. Rev. Lett. **82**(2), 450–452 (1999)

21. Thissen, R., Witasse, O., Dutuit, O., Wedlund, C.S., et al.: Phys. Chem. Chem. Phys. **13**, 18264–18287 (2011)
22. Alagia, M., Balucani, N., Candori, P., Falcinelli, S., Richter, R., et al.: Rendiconti Lincei Scienze Fisiche e Naturali **24**, 53–65 (2013)
23. Falcinelli, S., Rosi, M., Candori, P., Farrar, J.M., Vecchiocattivi, F., et al.: Planet. Space Sci. **99**, 149–157 (2014)
24. Falcinelli, S.: Acta Phys. Pol., A **131**(1), 112–116 (2017)
25. Ben Arfa, M., Lescop, B., Cherid, M., Brunetti, B., Candori, P., et al.: Chem. Phys. Lett. **308**, 71–77 (1999)
26. Brunetti, B.G., Candori, P., Ferramosche, R., Falcinelli, S., et al.: Chem. Phys. Lett. **294**, 584–592 (1998)
27. Pei, L., Carrascosa, E., Yang, N., Falcinelli, S., Farrar, J.M.: J. Phys. Chem. Lett. **6**(9), 1684–1689 (2015)
28. Falcinelli, S.: AIP Conference Proceedings, vol. 2075, p. 050003 (2019)
29. Bettoni, M., Candori, P., Falcinelli, S., Marmottini, F., Meniconi, S., Rol, C., Sebastiani, G. V.: J. Photochem. Photobiol., A **268**, 1–6 (2013)
30. Alagia, M., Candori, P., Falcinelli, S., Pirani, F., et al.: Phys. Chem. Chem. Phys. **13**(18), 8245–8250 (2011)
31. Alagia, M., Candori, P., Falcinelli, S., Lavollée, M., et al.: J. Chem. Phys. **126**(20), 201101 (2007)
32. Hotop, H., Illenberger, E., Morgner, H., Niehaus, A.: Chem. Phys. Lett. **10**(5), 493–497 (1971)
33. Brunetti, B.G., Candori, P., Cappelletti, D., Falcinelli, S., et al.: Chem. Phys. Lett. **539–540**, 19–23 (2012)
34. Bethe, H.A.: Phys. Rev. **57**, 1125–1144 (1940)
35. Falcinelli, S., Vecchiocattivi, F., Pirani, F.: Phys. Rev. Lett. **121**(16), 163403 (2018)
36. Falcinelli, S., Vecchiocattivi, F., Pirani, F.: J. Chem. Phys. **150**(4), 044305 (2019)
37. Balucani, N., Bartocci, A., Brunetti, B., Candori, P., et al.: Chem. Phys. Lett. **546**, 34–39 (2012)
38. Miller, W.H., Morgner, H.: J. Chem. Phys. **67**, 4923–4930 (1977)
39. Brunetti, B., Candori, P., Falcinelli, S., Pirani, F., Vecchiocattivi, F.: J. Chem. Phys. **139**(16), 164305 (2013)
40. Falcinelli, S., Candori, P., Pirani, F., Vecchiocattivi, F.: Phys. Chem. Chem. Phys. **19**(10), 6933–6944 (2017)
41. Alagia, M., Brunetti, B.G., Candori, P., Falcinelli, S., et al.: J. Chem. Phys. **120**(15), 6980–6984 (2004)
42. Alagia, M., Biondini, F., Brunetti, B.G., Candori, P., et al.: J. Chem. Phys. **121**(21), 10508–10512 (2004)
43. Candori, P., Falcinelli, S., Pirani, F., Tarantelli, F., Vecchiocattivi, F.: Chem. Phys. Lett. **436**, 322–326 (2007)
44. Lombardi, A., Lago, N.F., Laganà, A., Pirani, F., Falcinelli, S.: A bond-bond portable approach to intermolecular interactions: simulations for N-methylacetamide and carbon dioxide dimers. In: Murgante, B., et al. (eds.) ICCSA 2012. LNCS, vol. 7333, pp. 387–400. Springer, Heidelberg (2012). https://doi.org/10.1007/978-3-642-31125-3_30
45. Cappelletti, D., Bartocci, A., Grandinetti, F., Falcinelli, S., et al.: Chem. Eur. J. **21**(16), 6234–6240 (2015)
46. Alagia, M., Brunetti, B.G., Candori, P., Falcinelli, S., et al.: J. Chem. Phys. **120**(15), 6985–6991 (2004)
47. Alagia, M., et al.: J. Chem. Phys. **136**, 204302 (2012)

48. Teixidor, M.M., Pirani, F., Candori, P., Falcinelli, S., Vecchiocattivi, F.: Chem. Phys. Lett. **379**, 139–146 (2003)
49. Alagia, M., Brunetti, B.G., Candori, P., et al.: J. Chem. Phys. **124**(20), 204318 (2006)
50. Alagia, M., Candori, P., Falcinelli, S., Mundim, K.C., Mundim, M.S.P., Pirani, F., et al.: Chem. Phys. **398**, 134–141 (2012)
51. Cappelletti, D., Candori, P., Falcinelli, S., Albertì, M., Pirani, F.: Chem. Phys. Lett. **545**, 14–20 (2012)
52. Pirani, F., Maciel, G.S., Cappelletti, D., Aquilanti, V.: Int. Rev. Phys. Chem. **25**, 165–199 (2006)
53. Aquilanti, V., Luzzatti, E., Pirani, F., Volpi, G.G.: J. Chem. Phys. **89**(10), 6165–6175 (1988)
54. Aquilanti, V., Liuti, G., Pirani, F., Vecchiocattivi, F.: J. Chem. Soc., Faraday Trans. **85**(8), 955–964 (1989)
55. Tosi, P., et al.: J. Chem. Phys. **99**(2), 985–1003 (1993)
56. Bartocci, A., Belpassi, L., Cappelletti, D., Falcinelli, S., et al.: J. Chem. Phys. **142**(18), 184304 (2015)
57. Aquilanti, V., Cappelletti, D., Lorent, V., Pirani, F.: J. Phys. Chem. **97**, 2063–2071 (1993)
58. Krauss, M.: J. Chem. Phys. **67**(4), 1712–1719 (1977)
59. Brunetti, B., Candori, P., Falcinelli, S., Lescop, B., et al.: Eur. Phys. J. D **38**, 21–27 (2006)
60. Brunetti, B., Candori, P., De Andres, J., Pirani, F., Rosi, M., et al.: J. Phys. Chem. A **101** (41), 7505–7512 (1997)
61. Alagia, M., Boustimi, M., Brunetti, B.G., Candori, P., et al.: J. Chem. Phys. **117**(3), 1098–1102 (2002)
62. Alagia, M., Candori, P., Falcinelli, S., Mundim, M.S.P., Pirani, F., et al.: J. Chem. Phys. **135** (14), 144304 (2011)
63. Alagia, M., Bodo, E., Decleva, P., Falcinelli, S., et al.: Phys. Chem. Chem. Phys. **15**(4), 1310–1318 (2013)
64. Troiani, A., Rosi, M., Garzoli, S., Salvitti, C., de Petris, G.: Chem. Eur. J. **23**, 11752–11756 (2017)
65. Pirani, F., et al.: Angew. Chem. Int. Ed. **58**(13), 4195–4199 (2019)
66. Gordon, S.D.S., Omiste, J.J., Zou, J., Tanteri, S., Brumer, P., Osterwalder, A.: Nat. Chem. **10**, 1190–1195 (2018)
67. Gordon, S.D.S., Zou, J., Tanteri, S., Jankunas, J., Osterwalder, A.: Phys. Rev. Lett. **119**, 053001 (2017)
68. Skouteris, D., Balucani, N., Faginas-Lago, N., et al.: A&A **584**, A76 (2015)
69. Skouteris, D., Balucani, N., Ceccarelli, C., Faginas Lago, N., et al.: MNRAS **482**, 3567–3575 (2019)